

1 **Reanalysis Surface Mass Balance of the Greenland Ice Sheet along K-transect**
2 **(2000-2014)**

3 **Mahdi Navari^{1,2}, Steven A. Margulis³, Marco Tedesco^{4,5}, Xavier Fettweis⁶, and R.S.W. van**
4 **de wal⁷**
5

6 ¹University of Maryland Earth Systems Science Interdisciplinary Center and Hydrological
7 Sciences Laboratory, Collage park, MD, USA.

8 ²NASA Goddard Space Flight Center, Greenbelt, MD, USA.

9 ³Department of Civil and Environmental Engineering, University of California Los Angeles,
10 California.

11 ⁴Lamont Doherty Earth Observatory of Columbia University, Palisades, New York, NY.

12 ⁵NASA Goddard Institute for Space Studies, New York, NY, USA.

13 ⁶Department of Geography, University of Liège, Liège, Belgium.

14 ⁷Institute for Marine and Atmospheric research Utrecht and Department of Physical Geography,
15 Utrecht University, Netherlands

16 Corresponding author: Mahdi Navari (mahdi.navari@nasa.gov)
17

18 **Key Points:**

19 • **A data assimilation technique was used to generate a reanalysis estimates of the surface mass balance of the**
20 **Greenland ice sheet along the K-transect stations**

21 • **A particle batch smoother technique was used to condition the prior estimates of surface mass balance on**
22 **16-day MODIS albedo**

23 • **Results show that the assimilation of albedo reduces the RMSE of the surface mass balance estimates by**
24 **51%**

25
26

27 **Abstract**
28

29 Accurate estimates of surface mass balance over the Greenland ice sheet (GrIS) would
30 contribute to understanding the cause of recent changes and would help to better estimate the future
31 contribution of the GrIS to sea-level rise. Given the limitations of in-situ measurement, modeling,

32 and remote sensing, it is critical to explore the opportunity to merge the available data to better
33 characterize the spatial and temporal variation of the GrIS surface mass balance (SMB).

34 This work utilizes a particle batch smoother data assimilation technique that yields SMB
35 estimates that benefit from the snow model Crocus and a 16-day albedo product derived from
36 satellite remote sensing data. Comparison of the results against in-situ SMB measurements shows
37 that the assimilation of the albedo product reduces the root mean square error (RMSE) of the
38 posterior estimates of SMB by 51% and reduces bias by 95%.

39

40 **Plain Language Summary**

41 GrIS is losing mass through ice discharge from outlet glaciers and surface processes (e.g.,
42 meltwater runoff, sublimation, and evaporation). Recent studies suggest that meltwater runoff will
43 be the dominant mass loss process over the GrIS in the future as it will increase under climate
44 warming. Accurate estimates of the GrIS SMB are a critical objective, which, despite its
45 importance, continues to contain large uncertainties from significant errors in forcing data as well
46 as model errors. This work uses a data assimilation framework (which has not been used in
47 estimation of the GrIS SMB) and a satellite-derived 16-day albedo product to produce a reanalysis
48 estimates of SMB along the Kangerlussuaq transect (K-transect) stations in west Greenland. We
49 used the K-transect in-situ SMB measurements to validate our results over the 2000–2014
50 hydrological year. The data assimilation technique (i.e., particle batch smoother) reduces the
51 spatial root-mean-square error of SMB over the K-transect stations by 51% from 858 millimeter
52 water equivalent (mmWE) to 423 mmWE and the bias in the estimates by 95%, from -70 mmWE
53 to 3.5 mmWE. It was shown that this methodology has the potential to resolve the spatial
54 variability of the surface processes along the K-transect stations and in particular of the bare ice
55 surface albedo that is not resolved by the model at a resolution of 25 km (i.e., the model uses a
56 constant bare ice albedo). The results suggest that the methodology can be applied over the entire
57 GrIS using MODIS albedo observations to generate an improved reanalysis of SMB estimates.

58 **1. Introduction and background**

59 The Greenland ice sheet (GrIS) has been the focus of climate studies due to its considerable
60 impact on sea-level rise via net mass gain or loss (mass balance; MB). Surface mass balance (SMB)
61 and ice dynamics are the two mechanisms that control the overall MB. The former includes mass
62 loss/gain through surface processes, and the latter results from direct displacement of water by
63 glacial ice and basal melt. GrIS MB observations show that mass loss has been accelerating over
64 the last decade (e.g., Lenaerts et al., 2019, Mouginit et al., 2019). Van Angelen et al. (2013) and
65 Fettweis et al., (2013, 2017) highlighted that meltwater runoff is the dominant mass loss process
66 over the GrIS. Despite its importance, estimates of SMB over the GrIS contain significant
67 uncertainties (e.g., Rignot et al., 2011; Vernon et al., 2013; Fettweis et al., 2020).

68 The focus of this study is to further evaluate the proposed methodology on better constraining
69 SMB through surface processes via additional (indirect) observations and a data assimilation
70 framework. Numerical models offer a key tool for quantifying the GrIS surface mass fluxes.
71 However, modeling approaches are generally limited by uncertainty in meteorological forcing data
72 and model errors, which directly propagate into the model results (e.g., Vernon et al., 2013;
73 Fettweis et al., 2020). In-situ measurements such as the network of Kangerlussuaq transect (K-
74 transect) stations in west Greenland (Van de Wal et al., 2012; Smeets et al., 2018) offer valuable
75 information about SMB over the western ablation area. However, there is an extremely limited
76 number of in situ SMB data in the rest of GrIS.

77 Using surface remote sensing data is a practical alternative to in-situ measurements. Given the
78 spatial coverage, remote sensing data can partially address some of the issues related to the sparse
79 in situ measurements. Unfortunately, surface mass fluxes such as precipitation, evaporation, and
80 runoff cannot be directly measured via remote sensing. This makes the possibility of quantitatively
81 characterizing the surface mass fluxes from remote sensing retrieval algorithms difficult. Despite
82 this challenge, indirect or implicit relationships do exist between surface remote sensing
83 data/products and surface mass fluxes. Surface remote sensing data such as albedo, contains
84 valuable information about the GrIS surface features, including fresh snow, impurities in the
85 snowpack, the presence of liquid water, the formation of supraglacial lakes, and the exposure of
86 bare ice, among other things. However, albedo alone fails to provide quantitative information
87 about the surface mass fluxes.

88 Given the limitation of different individual methodologies, we argue that using a reanalysis–
89 type approach that merges relevant data streams from satellite observations with a physical model
90 can significantly improve the spatially and temporally continuous estimates of SMB over the GrIS.
91 Margulis et al. (2016) provided an example of a such approach to characterize thirty years of snow
92 water equivalent (SWE) over the Sierra Nevada (United States). We adopted that methodology for
93 a one-year proof of concept study (Navari et al. 2018) in the K-transect region in west Greenland.
94 This work is a continuation of our previous work by extending the study period from 2000 to 2014
95 (this period is based on the availability of the MAR v3.5 data; Fettweis et al., 2017). In this study,
96 we take advantage of the reanalysis approach to merge a 16-day albedo product with near-surface
97 meteorological forcing data and a snow model knowing that albedo variability is highly correlated
98 to the recent surface mass balance decrease (Riihelä et al., 2019). The reanalysis approach uses a
99 fully Bayesian data assimilation framework to merge different data streams (Margulis et al. 2015,
100 2016).

101 The primary difference between the previous studies and the one presented herein include the
102 fact that the previous studies focused primarily on estimating SMB via remote sensing (e.g.,
103 Enderlin et al., 2014) or modeling tools (e.g., Fettweis et al., 2017; Noël et al., 2018; Sellevold et
104 al., 2019) alone. Here, we use a data assimilation approach that does not rely on in-situ data and
105 integrates satellite observations into a snow model. To-date, there have been very limited studies
106 that used data assimilation to predict the GrIS MB/SMB components (e.g., Larour et al. 2014;
107 Navari et al. 2016; 2018).

108 The methodology described below is for estimating the SMB along the K-transect stations, but
109 the methodology is general and can be applied to larger domains where surface albedo
110 measurements are available. The primary objective of this paper is to present the SMB reanalysis
111 dataset, its validation, and an illustration of its utility in the context of quantifying the current GrIS
112 SMB. Methods and data are presented in section 2. The results are presented in section 3.
113 Discussion, conclusions, and implications for future work extending to the entire GrIS are
114 presented in section 4.

115 **2. Methods and data**

116 **2.1. Application domain**

117 The selected area is located near the city of Kangerlussuaq, in west Greenland along an east-
118 west transect (K-transect) close to the 67° N latitude. The transect has been equipped with different
119 observation instruments including automatic weather stations and SMB stakes at different
120 elevations. Seven SMB measurement stations (S4, S5, SHR, S6, S7, S8, and S9) are located in the
121 ablation zone, and the last station (S10) is located in the percolation zone (Van de Wal et al., 2012).
122 The station IDs and their spatial distribution within the MAR/Crocus 25 km² computational grid
123 cells are shown in Figure 1b.

124

125 **2.2. Reanalysis methodology**

126 The reanalysis method applied in this study consists of a particle batch smoother (PBS) data
127 assimilation approach developed and validated in Margulis et al. (2015, 2016) for seasonal
128 snowpack over the Sierra Nevada, and Navari et al. (2018) for a single year SMB along the K-
129 transect. The snowpack model Crocus (Vionnet et al. 2012) is used to generate uncertain prior
130 estimates of SMB and snow albedo over the study area. An effective way to significantly reduce
131 model and observational errors and produce superior estimates of SMB fluxes is to constrain the
132 snowpack model predictions with satellite observations through data assimilation methods.

133 There are many DA techniques to integrate model estimates with observations. Sequential DA
134 methods such as Ensemble Kalman Filter (EnKF) Kumar et al. (2017), and Particle Filter (PF)
135 Cluzet et al. (2021) are used for real-time application. Non-sequential DA methods such as
136 ensemble batch smoother (EnBS) and PBS are usually used for reanalysis. Margulis et al. (2016)
137 showed that PBS generally outperformed the EnBS because it provides optimal Bayesian
138 conditioning. For a more detailed discussion about the methodology, see supporting document text
139 S1.

140 The PBS ingests prior estimates from the snow model Crocus and remotely sensed 16-day
141 albedo observations. The approach generates an ensemble posterior SMB estimate over the study
142 domain. The data assimilation step consists of using the 16-day albedo misfit and the 16-day albedo
143 measurement error covariance to derive the posterior ensemble estimate via a likelihood function.
144 The likelihood function simply increases the weight of the replicates (particles) that are closer to

145 the observations and decreases the weights of the replicates that are further from the observations.
146 The updated weights are a discrete approximation of the posterior PDF which can be used to
147 directly estimate posterior statistics of the state variables. The PBS updates the states in a single
148 step using all measurements in the assimilation window. The PBS approach characterizes the
149 mean, median, variance and interquartile range of SMB. For a more detailed discussion about the
150 methodology, see supporting document text S1.

151

152 **2.3. Datasets used**

153 **a) Forcing data**

154 The data assimilation framework in this study uses hourly near-surface meteorological forcing
155 data (i.e., temperature, pressure, wind speed, longwave and shortwave radiation, precipitation,
156 humidity) and initial snow and ice profile from the regional climate model Modèle Atmosphérique
157 Régional (MAR; Gallée and Schayes 1994; Gallée and Duynkerke 1997) to force the offline
158 Crocus model. The regional climate model MAR is fully coupled with the snow physical model
159 Crocus. However, the integration of the MAR model in an ensemble mode would require
160 significant computational resources. Instead, in the reanalysis data assimilation system, we perturb
161 MAR output meteorology (i.e., temperature, longwave, shortwave, and precipitation) to generate
162 an ensemble of forcing that is passed to Crocus, which significantly reduces the computational
163 cost.

164

165 **b) Snow model Crocus**

166 In this study, we used a stand-alone version of Crocus (Crocus V24), which is different from
167 the version coupled with MAR. The albedo module in this version is simple, therefore, we have
168 updated the Crocus albedo module based on the MAR albedo as follows: the site-specific snow
169 aging term was removed from the visible snow albedo formulation, the lower limit of snow albedo
170 for all spectral ranges was set to 0.65, and the MAR snow and ice albedo transition equations were
171 used to ensure a smooth transition between snow and ice albedo. The more recent version of
172 Crocus is integrated into Meteo-France's SURFEX platform and it is available online at
173 https://opensource.umr-cnrm.fr/projects/snowtools_git/wiki.

174

175 **c) Remotely sensed albedo data**

176 MODIS 16-day albedo (MCD43A, Version-6; Schaaf, C., Wang, Z. 2015) is a high-quality
177 combined product that uses both Terra and Aqua data to provide 500 m albedo. The product
178 algorithm uses data from days 1 through to 16 to compute the albedo on day 9. We used the direct
179 and diffuse fraction of shortwave irradiance based on the algorithm by Allen et al., (2006) to
180 linearly combine black-sky albedo and white-sky albedo at local solar noon to obtain the true blue-
181 sky albedo that is most consistent with the model-generated albedo. Note that we aggregated the
182 raw albedo data to the model resolution of 25 km² and performed the data assimilation in the model
183 spatial resolution. The quality of albedo products decreases where the solar zenith angle is higher
184 than 70° (Stroeve et al. 2005, 2006). Therefore, all the observations corresponding to solar zenith
185 angles larger than 70° were removed from the data set.

186 Figures 1b-e show an illustration of the spatial and temporal evolution of albedo on May 9, June
187 10, July 12, and August 13, 2010, around the K-transect stations. As seen most clearly in panels b
188 and c, albedo gradually increases with elevation. Albedo is low along the margins of the ice sheet,
189 where the first three K-transect stations (S4, S5, and SHR) are located and gradually increases
190 eastward. The irregular variations (low albedo values) seen in panels d and e around -49° longitude
191 (known as the 'dark zone') are mainly driven by snow and ice impurities (e.g., Wientjes et al.,
192 2011, Ryan et al., 2018). During May and June, fresh snow has covered the impurities allowing
193 for a smooth east-west transition between high and low albedo. Temporal variations of albedo can
194 also be seen, most notably between May 9 and July 12. With the advancing melt season, snow
195 cover gradually disappears, and light-absorbing impurities significantly reduce the albedo. This
196 GrIS dark zone increases the absorbed solar radiation and consequently enhances the magnitude
197 of snow/ice melt. Hence, obtaining accurate estimates of snow/ice melt require incorporating this
198 information into model estimates.

199 200 **d) Verification data**

201 The data used for verification in this study are in situ SMB measurements obtained from eight
202 stations (SMB stakes) of differing elevations along the K-transect. Since 1990, SMB
203 measurements have been carried out at these locations in western Greenland (Van de Wal et al.,
204 2012; Smeets et al., 2018). This data set is the longest record of ground-based SMB measurements
205 in Greenland. The measurements and adjustment of the stakes were conducted in late August, first
206 days of September every year and all data have been quality controlled, reconstructed, and adjusted
207 as needed.

208

209 **e) A quantitative comparison of forward modeling approaches to characterize spatial and temporal**
210 **variation of the GrIS SMB**

211 Forward modeling is a commonly used methodology for providing spatially and temporally
212 continuous estimates of SMB over the GrIS (e.g., Fettweis et al., 2017; Noël et al., 2018; Sellevold
213 et al., 2019). Such deterministic methodologies differ from the work presented herein in several
214 important ways.

215 Offline forward modeling methodologies are generally limited by uncertainty in meteorological
216 forcing data and subject to direct propagation of errors in those forcings and model errors, both of
217 which impact the estimates of SMB over the GrIS (e.g., Vernon et al., 2013).

218 The novelty of the reanalysis dataset presented herein lies in the use of a fully probabilistic
219 Bayesian assimilation method and the use of information available in the satellite-derived albedo
220 data. The Bayesian PBS method leverages the information content of a meso-scale atmospheric
221 model (i.e., MAR) and the albedo to generate the best estimates of SMB, related fluxes, and their
222 corresponding uncertainty.

223 The application and characterization described in this research are meant to be illustrative of
224 potential future applications over the entire GrIS. The primary focus of this study was to use the
225 SMB reanalysis dataset to characterize the 15-year SMB in the K-transact in terms of its mean and
226 interannual variability. We will focus on comparing reanalysis results with the in-situ
227 measurements to explain basic changes in the SMB through space and time.

228 **3. Results**

229 The model setup and open-loop simulation are described in Navari et al. (2018). For this
230 simulation, we used MAR v3.5 (Fettweis et al., 2017) outputs for offline model inputs and we also
231 used a new set of albedo data (i.e., MCD43A, Version-6). The data assimilation was performed
232 over the 15 years between 2000 and 2014. To illustrate how the PBS data assimilation
233 methodology works, we first present results for a representative individual computational grid-cell
234 and then present time series of SMB for all computational grid cells.

235 The in-situ measurements sites are located within six MAR grid 25 km² cells. Two grid cells
236 contain two stations, three grid cells contain one station and there is no station in one grid cell
237 (Figure 1b). A preliminary analysis of in-situ SMB measurements (from 1990 to 2014) reveals that
238 more than 60 percent of the total mass loss along K-transect stations occurs within the first

239 computational grid cell from the edge of the ice sheet and more than 95% in the first two grid cells
240 (see Text S2 and Table S1 in the supporting information). Therefore, for illustrative purposes, the
241 focus will be on the first computational grid cell (co-located with the S5 and SHR stations). S5
242 and SHR located at 6 km and 14 km from the ice sheet margin respectively.

243 Figure 2 illustrates the time series of the 16-day albedo data during each year for the selected
244 computational grid cell for the study period (see Figure S1-S4 in the supporting information for
245 other grid-cells). Note that PBS applied to each grid cell sequentially with an assimilation window
246 of one year. The observations consist of the MODIS-derived 16-day albedo which are used to
247 condition the prior Crocus estimates in order to produce the posterior estimates. The prior and
248 posterior estimates are the 16-day albedo data from the Crocus snow model before and after the
249 assimilation of satellite-derived albedo. The ensemble statistical information such as the
250 interquartile range (IQR) and median are used to evaluate the accuracy of the estimates.

251 In the selected grid cell, the fresh and dry snow accumulated over the bare ice during the
252 previous accumulation season shows a very high albedo where the satellite-derived albedo remains
253 around 0.75 until mid-April (Figure 2). During the spring (April, May), the snowpack ages and
254 starts to melt, causing a decrease in albedo from 0.75 to around 0.40. During the summer (June-
255 August), the observed albedo remains almost constant at around 0.4. During this period, incoming
256 solar radiation contributes primarily to melting ice layers. The surface albedo increases again when
257 a new accumulation season starts in September.

258 As shown in Figure 2 (all panels), the prior albedo estimates (red dashed lines) are higher than
259 the satellite observations (green circles) over the entire simulation period, in agreement with
260 Alexander et al. 2014. These figures clearly show that the model overestimates the (bare ice)
261 albedo mainly due to inaccurate bare ice albedo parameterization, and a lack of parameterization
262 of impurities. The generally higher albedo implies that the ice sheet surface reflects more incoming
263 solar radiation into the atmosphere and consequently underestimates the snowmelt and ice melt.
264 The ensemble spread of the prior estimates is very large (the IQR ranges from around 0.4 to 0.85)
265 due to uncertain forcings.

266 The PBS uses the distance between the prior model estimates and observations to generate the
267 posterior estimates. As shown in Figure 2, by construct, assimilation of satellite observation moves
268 the posterior estimates (blue shaded areas and blue lines) toward the observations, and most of the
269 observations are within the ensemble spread. The PBS accomplishes this by more heavily

270 weighting ensemble members that more closely match the observations through the likelihood
271 function embedded in the PBS formulation. The blue dashed lines in Figure 2 are more in
272 agreement with the observations than are the prior estimates. The uncertainty of the posterior
273 estimates is considerably smaller than that of the prior estimates due to the fact that the PBS
274 reduces the weights of ensemble members that are far from the observations.

275 Figure 3 shows the SMB for all model grid cells along the K-transect. To be able to compare
276 the results with in-situ measurements at K-transect, we convert the time series of SMB to annual
277 cumulative SMB which starts from September 1st of each year until August 31 of the following
278 year (see Text S2 and Table S1 in the supporting information). Positive SMB values indicate a net
279 increase in mass, and negative values indicate net mass loss within a given year. The assimilation
280 of 16-day albedo data results in an updated ensemble of SMB estimates that are more consistent
281 with the observed albedo. As shown in Figure 3, the PBS generally improves the SMB: the
282 posterior estimates move toward the independent SMB observations. Averaging over all grid cells,
283 the PBS improves the SMB estimates by 51 percent for the simulation period of 2000 to 2014.

284 Although in many cases the posterior simulations appropriately match the K-transect
285 observations, in some instances, the PBS estimates are inaccurate. For example, the posterior SMB
286 values in Figure 3a are relatively smaller than observations (overestimating mass loss), and they
287 are relatively larger than observations in Figure 3d (underestimating mass loss) (see table S1 in
288 the supporting information for quantitative values over the simulation period). By construct, the
289 PBS attempts to fit the model albedo to the observation (Figure 2); however, whether this results
290 in an improvement in SMB estimates depends on the accuracy of Crocus albedo module and how
291 it is related to SMB and the other energy fluxes. Note that assimilation of albedo is not intended
292 to solve the model errors which are not associated with albedo. While the albedo module has been
293 updated to use the MAR albedo module, the prior simulation shows that there are considerable
294 differences between the model and observations, which may be due in part to the inadequacy of
295 the albedo module and the complex nonlinear relationship between albedo and SMB. Scatterplot
296 of predicted albedo (prior and posterior) and MODIS 16-day albedo (see Figure S5 in the
297 supporting information) shows that assimilation of MODIS albedo reduces bias by shifting the
298 median toward the observations and reduces the uncertainty as shown by the error bar. The scatter
299 plots suggest that PBS significantly improves the albedo estimates in the grid cells with dominant
300 melt processes (Figure S5a-h). Estimated SMB (both prior and posterior) and measured SMB in

301 the grid cell co-located with the S10 station are close to each other. Since the model error is not
302 significantly higher than the observation error, the PBS does not modify the prior estimates.

303 In the first computational grid cell, which is co-located with stations S5 and SHR, the PBS
304 improves the posterior estimates of SMB by an average of 18.4 percent (Figure 3a) over the
305 simulation period (2000 to 2014). Although the PBS significantly improved model albedo in this
306 grid cell and posterior estimates of albedo are in good agreement with the observations (Figure 2h-
307 j), it overestimates the SMB in several years, for example year 2008-2010 (Figure 3a). It is likely
308 an indication that the nonlinear relationship between the albedo and SMB is biased toward
309 overestimating of SMB when bare ice is exposed. In the grid cell co-located with stations S6 and
310 S7 the PBS improves the SMB by 64 percent relative to the mean of independent in situ
311 measurements (Figure 3b). In the grid cell co-located with stations S8 and S9. The PBS improves
312 the posterior SMB of these two grid cells by 61 and 60 percent respectively (Figure 3c and d). In
313 the grid cell co-located with station S10 (in the percolation zone) the prior SMB simulation is very
314 close to the in-situ observations (Figure 3e). The posterior simulation therefore shows similar
315 result as the prior. Note that the temporal variation of albedo in this station during the melt period
316 is very small (Figure 1b and c) and the difference between the observed albedo and the model
317 estimated albedo (Figure S4 in the supporting information) are significantly smaller over this
318 snow-dominated grid cell than it is over grid cells with mixed snow and bare ice exposure.
319 Therefore, there is limited information to be exploited by the PBS toward improving the SMB.

320 **4. Discussion and Conclusion**

321 The PBS data assimilation (reanalysis) method for estimating SMB using 15 years of MODIS
322 albedo data was applied over the several MAR computational grid cells along K-transect stations.
323 The main outcomes of this study are as follows:

324 The PBS considerably improves the posterior estimates of SMB over the prior estimates. While
325 the prior simulations overestimate the albedo and consequently underestimate the surface mass
326 balance, the posterior simulations result in albedo that closely match the satellite-derived albedo
327 and provides posterior SMB estimates that are in good agreement with the in-situ SMB
328 measurements. Indeed, the PBS reduces the RMSE of the SMB estimates by 51% and reduces bias
329 by 95%. This is an encouraging result because the grid cells are distributed across different mass
330 balance zones with different melt and accumulation processes.

331 Ensemble size and measurement error are two key inputs to the data assimilation methodology
332 (Margulis et al. 2016). A sensitivity analysis (see Text S3 in the supporting information) showed
333 that by increasing the number of ensembles from 50 to 300 (computational cost increases by 600%)
334 the RMSE of the SMB estimates improves by 8%. These results support the argument that an
335 ensemble size of N=100 replicates seems sufficient for SMB reanalysis in this study.

336 The measurement error indicates the degree of trust in the observation relative to the prior
337 estimates. The sensitivity analysis on measurement error (see Text S4, Table S2, Figure S6-S7 in
338 the supporting information) showed that the posterior ensemble collapses when using small
339 measurement error. This means one ensemble member (the best fit) gets weight 1 and the rest of
340 the weights are very close to zero. Based on results from the sensitivity analysis a measurement
341 error standard deviation of 0.2 provides the best results. Considering the fact that the dynamic
342 range of albedo is between 0.8 for fresh snow to around 0.3 for bare ice, a measurement error of
343 0.2 is not unrealistic.

344 A close examination of the primary results shows that some ensemble members in the grid cells
345 close to the ice sheet margin do not experience the exposure of bare ice during the summer.
346 Therefore, time series of summertime albedo show bimodal distributions wherein the ensemble
347 members experiencing bare ice exposure cluster around a model-defined ice albedo and other
348 ensemble members cluster around a typical snow albedo value. These bimodal distributions result
349 in the PBS failing to find a robust fit. To mitigate this issue and smooth transition between the
350 replicates, each ensemble member uses a different, randomly assigned ice albedo between 0.35
351 and 0.65 instead of a constant ice albedo. This strategy results in intermediate albedo values when
352 grid cells contain a combination of snow and ice during the summertime. A combination of a
353 continuous transition between the ensemble members and higher measurement error help to
354 prevent ensemble collapse and provides a robust fit to observations (Figure 2).

355 Results presented in this work are obtained by comparing the SMB of the grid cells with the in-
356 situ SMB measurements at K-transect stations. As described above, there are two SMB stations in
357 each of the first two model grid cells from the edge of the ice sheet along the K-transect and above
358 95% of the SMB along the K-transect happens in these two grid cells. Therefore, using
359 observations from two in-situ stations over relatively flat topography with moderate slope can
360 significantly reduce the error of evaluation (i.e., point scale verses grid cell scale). However, we

361 acknowledge that in-situ point scale measurements may not be adequate for comparison against
362 model grid cells of 25 km².

363 Results from the proof-of-concept study (Navari et al., 2018) and results presented in this work
364 suggest that using the PBS framework is an alternative solution for improving estimates of SMB
365 over the traditional deterministic modeling solutions or pure remote sensing solutions. The results
366 also suggest that the methodology can be applied over the entire GrIS using MODIS albedo
367 observations (improving in particular the bare ice albedo value used by the model) to generate an
368 improved reanalysis of SMB estimates. It should also be highlighted that the reanalysis framework
369 presented in this work is a general framework and could, therefore, be utilized over other domains
370 such as the Antarctica ice sheet or mountainous glaciers. Finally, it is also important to note, that
371 in view of the sensitivity of the model-based SMB estimations to the used bare ice albedo, a mean
372 MODIS based bare ice albedo is notably used in RACMO in the aim of improving its SMB
373 estimation (Noël et al., 2016).

374

375 **Data Availability Statement**

376 The MODIS datasets were downloaded from
377 https://lpdaac.usgs.gov/dataset_discovery/modis/modis_products_table. All preprocessing and
378 data assimilation codes and evaluation data are available at
379 <http://www.hydroshare.org/resource/a8c5e72010064d3cb52522463fb42a9b>.

380

381 **Acknowledgement**

382 This work was partially sponsored by NASA through grant 80NSSC19K0304.

383

384 **Reference**

385

386 Alexander PM, Tedesco M, Fettweis X, van de Wal RSW, Smeets CJPP, van den Broeke MR.
387 Assessing spatiotemporal variability and trends in modelled and measured Greenland ice sheet
388 albedo (2000–2013). *Cryosphere*. 2014;8:2293–312. <https://doi.org/10.5194/tc-8-2293-2014>

389

390 Allen, R. G., Trezza, R., & Tasumi, M. (2006). Analytical integrated functions for daily solar
391 radiation on slopes. *Agricultural and Forest Meteorology*, 139(1), 55–73.
392 <https://doi.org/10.1016/j.agrformet.2006.05.012>

393

394 Brun, E., David, P., Sudul, M. & Brunot, G. (1992). A numerical model to simulate snow-cover
395 stratigraphy for operational avalanche forecasting, *J. Glaciol.*, 38(128), 13–22.
396 <https://doi.org/10.3189/S0022143000009552>

397

398 Enderlin, E. M., Howat, I. M., Jeong, S., Noh, M.-J., van Angelen J. H., & van den Broeke, M.
399 R. (2014). An improved mass budget for the Greenland ice sheet. *Geophys. Res. Lett.*, 41, 866–
400 872. <https://doi.org/10.1002/2013GL059010>

401

402 Fettweis, X., Franco, B., Tedesco, M., van Angelen, J. H., Lenaerts, J. T. M., van den Broeke, M.
403 R. & Gallée, H. (2013). Estimating the Greenland ice sheet surface mass balance contribution to
404 future sea level rise using the regional atmospheric climate model MAR, *Cryosph.*, 7(2), 469–
405 489, <https://doi.org/10.5194/tc-7-469-2013>

406

407 Fettweis, X., Box, J. E., Agosta, C., Amory, C., Kittel, C., Lang, C., ... Gallée, H. (2017).
408 Reconstructions of the 1900-2015 Greenland ice sheet surface mass balance using the regional
409 climate MAR model. *Cryosphere*, 11(2), 1015–1033. <https://doi.org/10.5194/tc-11-1015-2017>

410

411 Fettweis, X., Hofer, S., Krebs-Kanzow, U., Amory, C., Aoki, T., Berends, C. J., Born, A., Box, J.
412 E., Delhasse, A., Fujita, K., Gierz, P., Goelzer, H., Hanna, E., Hashimoto, A., Huybrechts, P.,
413 Kapsch, M.-L., King, M. D., Kittel, C., Lang, C., Langen, P. L., Lenaerts, J. T. M., Liston, G. E.,
414 Lohmann, G., Mernild, S. H., Mikolajewicz, U., Modali, K., Mottram, R. H., Niwano, M., Noël,
415 B., Ryan, J. C., Smith, A., Streffing, J., Tedesco, M., van de Berg, W. J., van den Broeke, M.,
416 van de Wal, R. S. W., van Kampenhout, L., Wilton, D., Wouters, B., Ziemen, F., and Zolles, T.:
417 GrSMBMIP: intercomparison of the modelled 1980–2012 surface mass balance over the
418 Greenland Ice Sheet, *The Cryosphere*, 14, 3935–3958, <https://doi.org/10.5194/tc-14-3935-2020> ,
419 2020.

420

421 Gallée, H. & Duynkerke, P. (1997). Air-snow interactions and the surface energy and mass
422 balance over the melting zone of west Greenland during the Greenland Ice Margin Experiment.
423 *Journal of Geophysical Research Atmospheres*, 102(D12), 13813–13824.
424 <https://doi.org/10.1029/96JD03358>

425

426

427 Gallée, H. & Schayes, G. (1994) Development of a Three-Dimensional Meso- γ Primitive
428 Equation Model: Katabatic Winds Simulation in the Area of Terra Nova Bay, Antarctica, *Mon.*

429 *Weather Rev.*, 122(4), 671–685, [https://doi.org/10.1175/1520-](https://doi.org/10.1175/1520-0493(1994)122<0671:DOATDM>2.0.CO;2)
430 [0493\(1994\)122<0671:DOATDM>2.0.CO;2](https://doi.org/10.1175/1520-0493(1994)122<0671:DOATDM>2.0.CO;2)
431
432 Larour, E., Utke, J., Csatho, B., Schenk, A., Seroussi, H., Morlighem, M., Rignot, E., Schlegel,
433 N., and Khazendar, A. (2014) : Inferred basal friction and surface mass balance of the Northeast
434 Greenland Ice Stream using data assimilation of ICESat (Ice Cloud and land Elevation Satellite)
435 surface altimetry and ISSM (Ice Sheet System Model), *Cryosph*, 8, 2335-2351,
436 <https://doi.org/10.5194/tc-8-2335-2014>
437
438 Lenaerts, J. T. M., Medley, B., van den Broeke, M. R., & Wouters, B. (2019). Observing and
439 Modeling Ice Sheet Surface Mass Balance. *Reviews of Geophysics*, 57(2), 376–420.
440 <https://doi.org/10.1029/2018RG000622>
441
442 Margulis, S. A., Cortés, G., Giroto, M., & Durand, M. (2016). A landsat-era Sierra Nevada snow
443 reanalysis (1985-2015). *Journal of Hydrometeorology*, 17(4), 1203–1221.
444 <https://doi.org/10.1175/JHM-D-15-0177.1>
445
446 Margulis, S., Giroto, M., Cortés, G. & Durand, M. (2015) A Particle Batch Smoother Approach
447 to Snow Water Equivalent Estimation, *J. Hydrometeorol.*, 150504130725006.
448 <https://doi.org/10.1175/JHM-D-14-0177.1>
449
450 Mouginot, J., Rignot, E., Bjørk, A. A., van den Broeke, M., Millan, R., Morlighem, M., Noël, B.,
451 Scheuchl, B., and Wood, M.: Forty-six years of Greenland Ice Sheet mass balance from 1972 to
452 2018, *Proceedings of the National Academy of Sciences*,
453 <https://doi.org/10.1073/pnas.1904242116>, 2019.
454
455 Navari, M., Margulis, S., Bateni, S. M., Tedesco, M., Alexander, P. & Fettweis, X. (2016).
456 Feasibility of improving a priori regional climate model estimates of Greenland ice sheet surface
457 mass loss through assimilation of measured ice surface temperatures, *Cryosph.*, 10(1), 103–120.
458 <https://doi.org/10.5194/tc-10-103-2016>
459
460 Navari, M., Margulis, S. A., Tedesco, M., Fettweis, X., & Alexander, P. M. (2018). Improving
461 Greenland Surface Mass Balance Estimates Through the Assimilation of MODIS Albedo: A
462 Case Study Along the K-Transect. *Geophysical Research Letters*, 45(13), 6549–6556.
463 <https://doi.org/10.1029/2018GL078448>
464
465 Noël, B., van de Berg, W. J., Machguth, H., Lhermitte, S., Howat, I., Fettweis, X., and van den
466 Broeke, M. R.: A daily, 1 km resolution data set of downscaled Greenland ice sheet surface mass
467 balance (1958–2015), *The Cryosphere*, 10, 2361–2377, <https://doi.org/10.5194/tc-10-2361-2016>
468
469 Noël, B., van de Berg, W. J., van Wessem, J. M., van Meijgaard, E., van As, D., Lenaerts, J. T.
470 M., Lhermitte, S., Kuipers Munneke, P., Smeets, C. J. P. P., van Ulf, L. H., van de Wal, R. S.
471 W., and van den Broeke, M. R.: Modelling the climate and surface mass balance of polar ice
472 sheets using RACMO2 –Part 1: Greenland (1958–2016), *The Cryosphere*, 12, 811–831,
473 <https://doi.org/10.5194/tc-12-811-2018>
474

475 Riihelä, A., King, M. D., and Anttila, K.: The surface albedo of the Greenland Ice Sheet between
476 1982 and 2015 from the CLARA-A2 dataset and its relationship to the ice sheet's surface mass
477 balance, *The Cryosphere*, 13, 2597–2614, <https://doi.org/10.5194/tc-13-2597-2019>, 2019
478

479 Rignot, E., Velicogna, I., van den Broeke, M. R., Monaghan, A. & Lenaerts, J. T. M. (2011).
480 Acceleration of the contribution of the Greenland and Antarctic ice sheets to sea level rise,
481 *Geophys. Res. Lett.*, 38, L05503. <https://doi.org/10.1029/2011GL046583>
482

483 Ryan, J. C., Hubbard, A., Stibal, M., Irvine-Fynn, T. D., Cook, J., Smith, L. C., ... Box, J.
484 (2018). Dark zone of the Greenland Ice Sheet controlled by distributed biologically-active
485 impurities. *Nature Communications*, 9(1), 1–10. <https://doi.org/10.1038/s41467-018-03353-2>
486

487 Schaaf, C., Wang, Z. MCD43A4 MODIS/Terra+Aqua BRDF/Albedo Nadir BRDF Adjusted Ref
488 Daily L3 Global - 500m V006 [Data set]. NASA EOSDIS Land Processes DAAC. Accessed
489 2021-05-29. <https://doi.org/10.5067/MODIS/MCD43A4.006> , 2015
490

491 Sellevold, R., Kampenhout, L. van, Lenaerts, J. T., Noël, B., Lipscomb, W., & Vizcaino, M.
492 (2019). Surface mass balance downscaling through elevation classes in an Earth System Model:
493 analysis, evaluation and impacts on the simulated climate. *The Cryosphere Discussions*, 6, 1–25.
494 <https://doi.org/10.5194/tc-2019-122>
495

496 Smeets, P. C. J. P., Kuipers Munneke, P., van As, D., van den Broeke, M. R., Boot, W.,
497 Oerlemans, H., ... van de Wal, R. S. W. (2018). The K-transect in west Greenland: Automatic
498 weather station data (1993–2016). *Arctic, Antarctic, and Alpine Research*, 50(1).
499 <https://doi.org/10.1080/15230430.2017.1420954>
500

501
502 van Angelen, J. H., van den Broeke, M. R., Wouters, B., & Lenaerts, J. T. M. (2013).
503 Contemporary (1960–2012) Evolution of the Climate and Surface Mass Balance of the
504 Greenland Ice Sheet. *Surveys in Geophysics*, 35(5), 1155–1174. [https://doi.org/10.1007/s10712-](https://doi.org/10.1007/s10712-013-9261-z)
505 [013-9261-z](https://doi.org/10.1007/s10712-013-9261-z)
506

507 Van de Wal, R. S. W., Boot, W., Smeets, C. J. P. P., Snellen, H., van den Broeke, M. R. &
508 Oerlemans, J. (2012). Twenty-one years of mass balance observations along the K-transect, West
509 Greenland, *Earth Syst. Sci. Data*, 4(1), 31–35. <https://doi.org/10.5194/essd-4-31-2012>
510

511 Vernon, C. L., Bamber, J. L., Box, J. E., van den Broeke, M. R., Fettweis, X., Hanna, E., &
512 Huybrechts, P. (2013). Surface mass balance model intercomparison for the Greenland ice sheet.
513 *The Cryosphere*, 7(2), 599–614. <https://doi.org/10.5194/tc-7-599-2013>
514

515 Wientjes, I. G. M., Van de Wal, R. S. W., Reichert, G. J., Sluijs, A. & Oerlemans, J. (2011). Dust
516 from the dark region in the western ablation zone of the Greenland ice sheet, *Cryosph.*, 5(3),
517 589–601. <https://doi.org/10.5194/tc-5-589-2011>
518

519
520

521

522

523

524
525
526
527
528
529
530
531
532
533
534
535
536
537
538
539
540
541
542
543
544
545
546
547
548
549
550
551
552

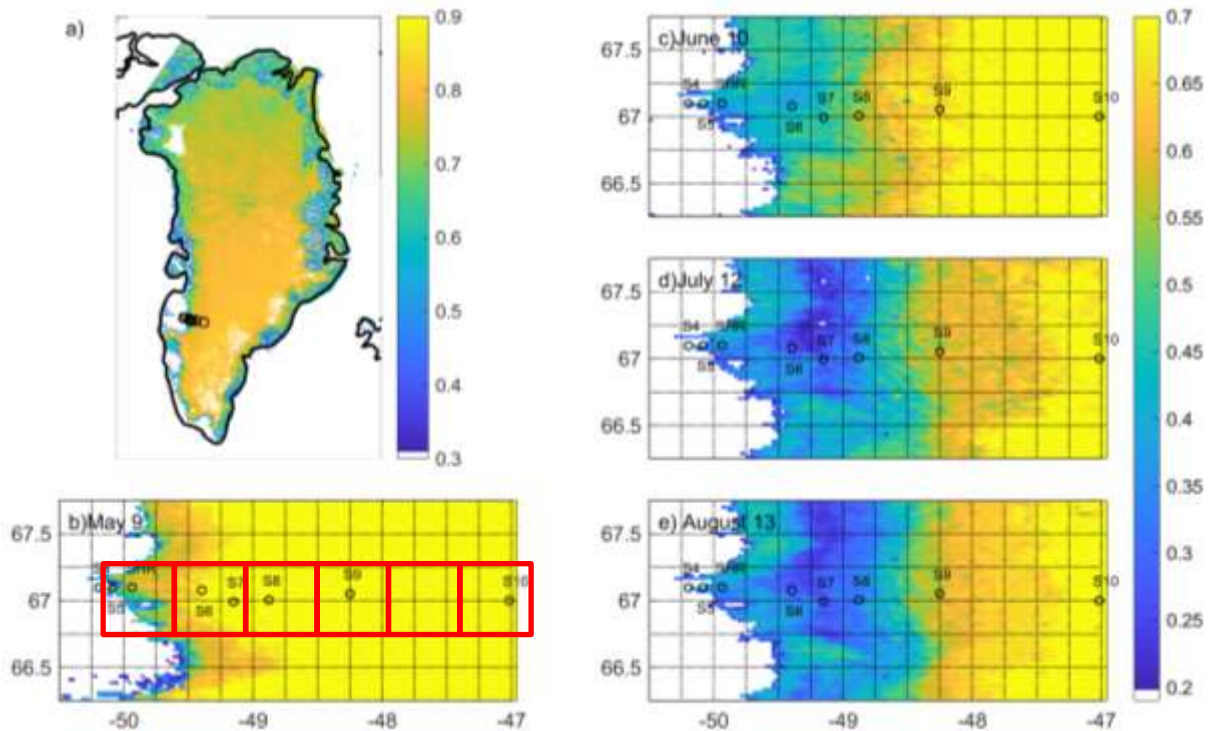
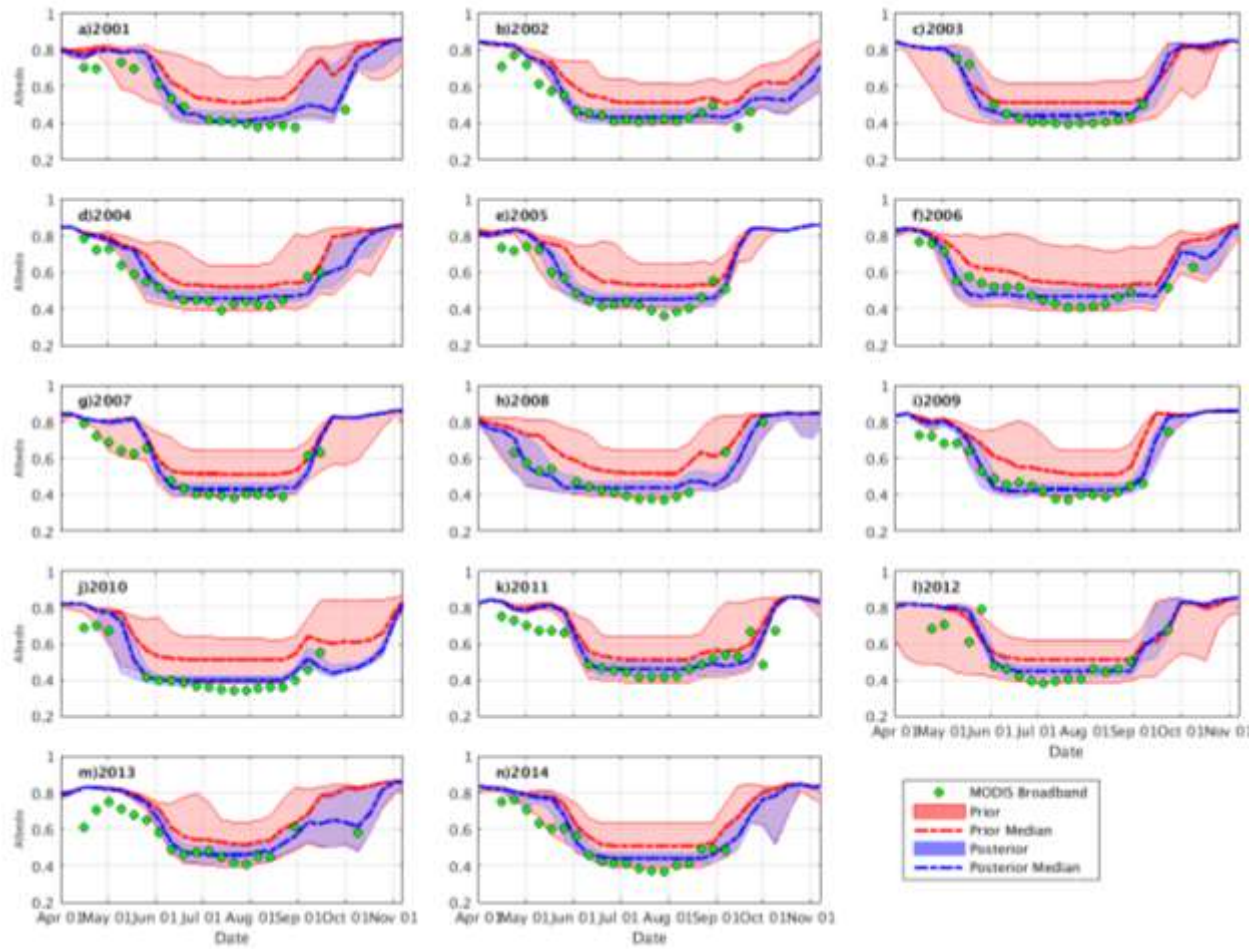


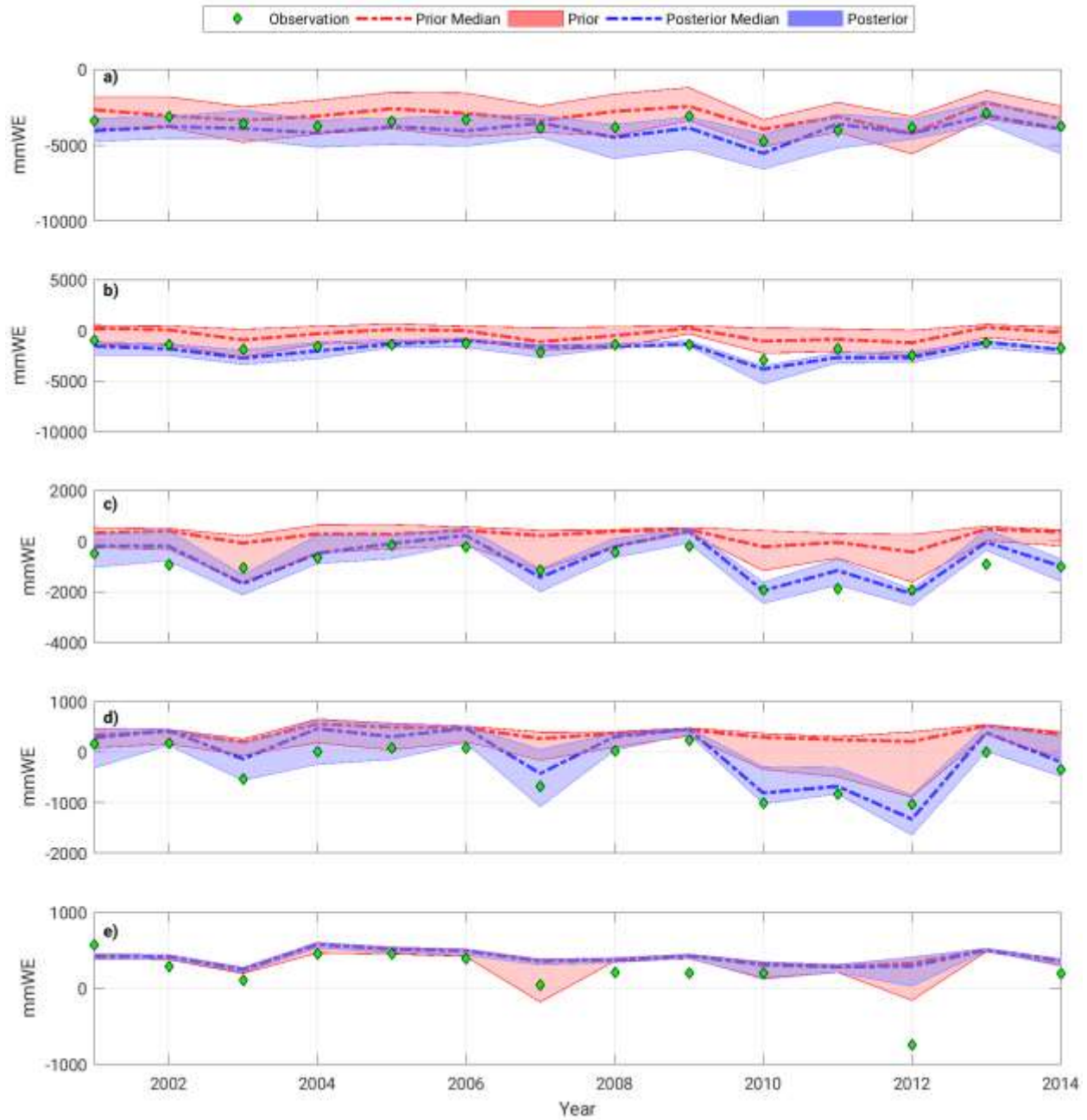
Figure 1: The 2010 16-day albedo map for (a) May 9 and a detailed map showing the location of K-transect stations, day of year (b) May 9, (c) June 10, (d) July 12, and (e) August 13. The black circles show the location of the K-transect stations S4, S5, SHR, S6, S7, S8, S9, and S10 respectively. The dark blue areas near S6-S8 in d-e represent the Greenland dark zone. The MAR/Crocus computational grid cell are shown in red in panel b.



553

554 **Figure 2: Time series of albedo (-) for the grid cell co-located with stations S5 and SHR for 2001 to**
 555 **2014. The red and blue shaded areas represent the prior and the posterior uncertainty band (IQR)**
 556 **and the red and blue dash lines represent the median of the prior and posterior, respectively. The**
 557 **green circles represent the satellite-derived 16-day albedo.**

558



559

560 **Figure 3: time series of the SMB for grid-cell co-located with the a) S5 and SHR, b) S6 and S7, c) S8,**
 561 **d) S9, and e) S10 stations along the K-transect. Values indicate year-over-year losses or gains in**
 562 **millimeter water equivalent (mmWE). The prior and posterior estimates are shown in red and blue,**
 563 **and in-situ SMB estimates along the K-transect are shown with green diamond.**